Ubiquitous Non-Majorana Zero-Bias Conductance Peaks in Nanowire Devices

J. Chen,[1,2] B. D. Woods,[3] P. Yu,[1] M. Hocevar,[4] D. Car,[5] S. R. Plissard,[6]
E. P. A. M. Bakkers,[5] T. D. Stanescu,[3] and S. M. Frolov[1,*]
[1]Department of Physics and Astronomy, University of Pittsburgh, Pittsburgh, Pennsylvania 15260, USA
[2]Department of Electrical and Computer Engineering and Peterson Institute of NanoScience and Engineering, University of Pittsburgh, Pittsburgh, Pennsylvania 15261, USA
[3]Department of Physics and Astronomy, West Virginia University, Morgantown, West Virginia 26506, USA
[4]Univ. Grenoble Alpes, CNRS, Grenoble INP, Institut Néel, 38000 Grenoble, France
[5]Eindhoven University of Technology, 5600 MB, Eindhoven, Netherlands
[6]LAAS CNRS, Université de Toulouse, 31031 Toulouse, France

(Received 8 February 2019; published 6 September 2019)

We perform tunneling measurements on indium antimonide nanowire-superconductor hybrid devices fabricated for the studies of Majorana bound states. At finite magnetic field, resonances that strongly resemble Majorana bound states, including zero-bias pinning, become common to the point of ubiquity. Since Majorana bound states are predicted in only a limited parameter range in nanowire devices, we seek an alternative explanation for the observed zero-bias peaks. With the help of a self-consistent Poission-Schrödinger multiband model developed in parallel, we identify several families of trivial subgap states that overlap and interact, giving rise to a crowded spectrum near zero energy and zero-bias conductance peaks in experiments. These findings advance the search for Majorana bound states through improved understanding of broader phenomena found in superconductor-semiconductor systems.

DOI: 10.1103/PhysRevLett.123.107703

Majorana bound states (MBS) are predicted in various intrinsic and engineered topological superconductors [1–7]. They attract sustained attention primarily thanks to the hypothesized non-Abelian rules for the two-MBS exchange [8]. Tunneling experiments reported signatures of MBS by studying zero-bias conductance peaks (ZBP) [9–21]. The primary challenge for the tunneling evidence is that zero-bias anomalies in transport are widespread in mesoscopic systems. They have many known non-MBS origins such as the Kondo effect [22], weak antilocalization [23], reflectionless tunneling [24], and supercurrent [25]. Luckily, most of these phenomena can be ruled out for each particular Majorana experiment through their distinct dependence on the *in situ* tunable parameters or through device design.

Yet, zero-bias anomalies of nontopological origin that closely resemble MBS, and cannot be straightforwardly ruled out, have also been identified. Most remarkably, trivial Andreev bound states (ABS) have been demonstrated to result in zero-bias peaks [26]. This includes peaks that appear at finite magnetic field and exhibit some degree of pinning to zero bias or near-zero oscillations, both being features that MBS and ABS share. Trivial ABS can exist both in the topologically superconducting regime and in the trivial regime, or they can be a result of strong MBS hybridization [27–29]. Thus ABS can be found in a much wider range of system parameters than MBS. Understanding of the full ABS phenomenology is therefore central to the unambiguous demonstration of MBS.

In this Letter, we demonstrate that multiple coexisting and coupled ABS can lead to ubiquitous zero-bias peaks that share spectroscopic signatures with MBS. Our NbTiN/InSb devices have been designed for Majorana experiments, and they yield tunneling resonances that pin near zero source-drain voltage bias at finite external magnetic field, as expected for MBS. However, extended gate voltage sweeps reveal multiple families of states localized near the superconductor. We identify these states as being responsible for the omnipresent zero-bias resonances. The frequency of occurrence of zero-bias features, i.e., their ubiquity, makes it highly unlikely that all of them originate from topologically superconducting segments of the nanowire. A self-consistent multiband model developed in parallel [30] finds a generic presence of overlapping and coupled trivial ABS for the device geometry used in the experiment. The model identifies that trivial ABS can persist near zero bias due to spectral crowding as well as level repulsion.

The basic MBS theories make a number of simple predictions for the tunneling manifestations of MBS in spin-orbit nanowires [4,5]. In long quantum wires MBS should only appear within the topologically superconducting phase described by the boundary equation, $E_Z > \sqrt{\Delta^2 + \mu^2}$, where $E_Z = g\mu_B B/2$ is the Zeeman energy, with g being the effective Landé g factor and μ_B the Bohr magneton. Δ is the induced superconducting gap at $B = 0$, and μ is the chemical potential in the quantum

wire. In the limits of zero temperature, hard induced gap, and weak tunnel coupling, MBS manifest as a $2e^2/h$ peak in conductance at zero tunneling bias. The peak emerges after the bulk superconducting gap in the nanowire closes and reopens. Beyond the reopening point the peak is robust—meaning it does not deviate from zero bias until superconductivity is fully suppressed by external field or another sub-band crosses the Fermi level. MBS come in pairs, and therefore a correlated zero-bias peak should be observed on the opposite end of the nanowire. Spin-orbit anisotropy implies that zero-bias peaks should vanish for a specific magnetic field orientation that is collinear with the effective spin-orbit field.

The demonstration of all of the above basic tunneling predictions in the same nanowire will likely amount to proof of Majorana bound states beyond reasonable doubt. To date, this has not been possible, despite steady progress in growth and fabrication [31–33]. A given device can be tuned to display one or more tunneling signatures of MBS but not to simultaneously confirm all of the basic expectations. The discrepancies may still be consistent with MBS but ascribed to experimental limitations such as finite temperature, soft induced gap, disorder, short nanowire length, and critical field anisotropy. When experimental limitations are accounted for, MBS are expected to result in conductance peak oscillations around zero bias, reduced peak height, no gap closing, and/or reopening and distorted topological phase boundary. As noted above, several theories and experiments furthermore point out that these features are shared between imperfect MBS and trivial ABS making the two effects challenging to distinguish. In this manuscript we study the phenomenology of low-bias resonances without assuming MBS, but with a goal of deeper understanding of the superconductor-semiconductor hybrid system.

Devices are fabricated using InSb semiconductor nanowires with NbTiN contacts (nominally identical to that used in [17], though device-to-device variations are common [Fig. 1(a); see Supplemental Material for additional devices]. Prior to the deposition of NbTiN, sulfur passivation is carried out followed by a gentle Ar plasma cleaning in order to obtain a transparent superconductor-semiconductor interface. A normal metal Pd contact is then fabricated to perform tunneling spectroscopy by varying bias voltage V between normal and superconducting contacts. Electrical measurements are performed in a dilution refrigerator at a base temperature of 30 mK, by a standard low-frequency lock-in technique (see detailed measurement conditions in Supplemental Material).

The electrostatic coupling of gates to the nanowire is enhanced due to half-coverage of the nanowire by the superconductor, as well as the use of a thin layer of high-κ gate dielectric (HfO_2, 10 nm). The gate effect is much stronger than in fully covered nanowires [18], or where side gates and/or thicker dielectric layers are used [9,34].

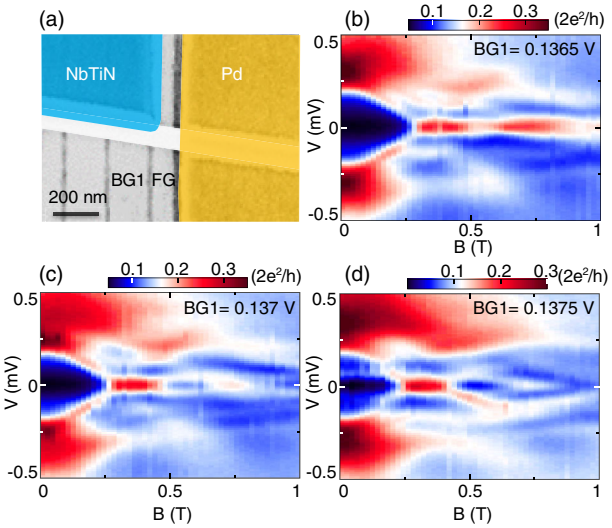

FIG. 1. (a) Scanning electron micrograph of the studied device. The bottom gates FG (100 nm wide) and BG1 (200 nm wide) are made of Ti(5 nm)/Au(10 nm). The nanowire is about 100 nm in diameter. The superconducting contact is a trilayer of Ti(5 nm)/NbTi(5 nm)/NbTiN(150 nm), while the normal contact is a Ti(15 nm)/Pd(150 nm) stack. [(b)–(d)] Differential conductance maps in bias voltage V versus magnetic field at BG1 = 0.1365, 0.137, and 0.1375 V, respectively. FG = 0.53 V for data in Figs. 1 and 2.

Stronger electrostatic coupling allows us to tune the density underneath the superconductor in a wider range, and observe a larger variety of subgap states as shown below. On the flip side, partial coverage may result in weaker induced superconductivity and soft gap [35]. Following a standard procedure for Majorana experiments [9], we create a single tunnel barrier between the normal and superconducting contacts by tuning gate FG (once set FG remains fixed). The gates left of BG1 are set to large negative voltages (−2.5 V) and not changed during the measurements. Those gates have no significant effect on the subgap states studied here.

We explore the magnetic field evolution of tunneling conductance in Figs. 1(b)–1(d). At zero field, this device exhibits a soft but otherwise featureless superconducting gap characterized by smooth evolution of suppressed conductance within the gap as a function of bias. Such a soft gap presents a decoherence pathway for futuristic topological qubits but it does not prevent us from studying the subgap spectroscopy here. In Fig. 1(b), the evolution within the magnetic field range 0–300 mT looks like a closing of the induced gap: the suppressed conductance window around zero bias shrinks and two branches of high conductance move from the apparent induced gap edges ($V = \pm 250\ \mu$V) toward lower bias reaching zero bias at around 300 mT. Beyond $B = 300$ mT, an apparent zero-bias resonance is observed over a significant range of magnetic field, up to at least $B = 1$ T. This range, expressed in Zeeman energy using a lower bound on

InSb g factor of 30, greatly exceeds the bias width of that resonance—thus we identify it as "pinned" to zero energy (line traces in Fig. S1 of Supplemental Material).

Figure 1(c) shows that with a minor variation in BG1 a single zero-bias resonance can be transformed into a pair of low-bias resonances oscillating around zero bias as magnetic field is increased to 1 T (up to 2 T in Supplemental Material). Such oscillations are consistent with MBS in a short nanowire [36], and in fact data in Fig. 1(b) can also be interpreted as similar oscillations of smaller amplitude, less than the resonance width. Figure 1(d), however, conveys a different picture. After another change in BG1 that should not alter the bulk density in any significant way, we can resolve that the apparent oscillations are actually superimposed of two unrelated pairs of resonances moving to zero bias at different magnetic fields, 0.4 and 0.7 T. This demonstrates that the visibility of different branches can be strongly affected by minor changes in gate voltages, and some of the branches may become invisible in color maps, creating the appearance of a sole zero bias resonance or a pair of oscillating resonances, both being important signatures of MBS.

The ubiquity of zero-bias features like those in Fig. 1 is demonstrated in Fig. 2. Because of the extended range of BG1 shown and because of the strong electrostatic coupling of BG1 to the nanowire, a large number of transient resonances can be seen crisscrossing the subgap region without sticking to zero bias at zero field [Fig. 2(a)]. These are due to states localized near the tunneling barrier. At finite magnetic field $B = 0.3$ T, the transient resonances are still visible, but another set of features tightly confined close to zero bias is now observed throughout the presented range of BG1 [Fig. 2(b)]. Close to 30 distinct ZBP regions are observed. If all of these ZBPs were due to topological

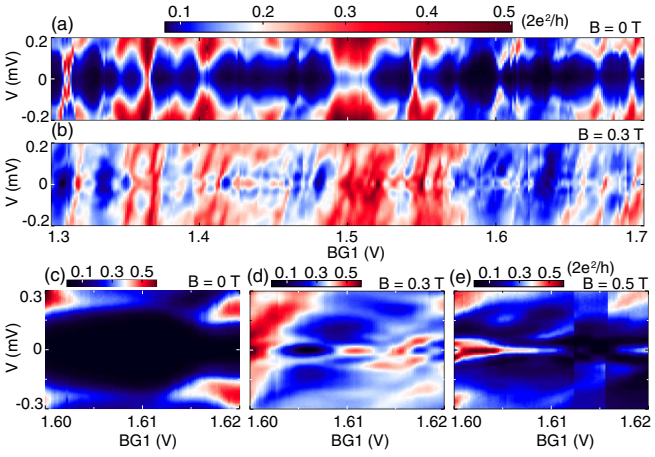

FIG. 2. Ubiquitous ZBP in extended range of gate BG1. [(a) and (b)] Differentiate conductance maps in bias voltage V versus BG1 at $B = 0$ and 0.3 T, respectively. [(c)–(e)] Differentiate conductance maps in bias voltage V versus BG1 in a small range at $B = 0$, 0.3 and 0.5 T, respectively.

superconductivity, we would expect being able to tune through tens of 1D sub-bands, which is inconsistent with quantum point contact measurements on similar nanowires [37]. Data in Fig. 2(b) are similar to barrier gate scans in Mourik *et al.* [9], which used the same nanowires and superconductors, though a different gate layout with a weaker BG1 coupling.

We zoom in on a representative BG1 range in Figs. 2(c)–2(e). At zero field the inside of the induced gap for $|V| < 250$ μV is featureless on this scale [Fig. 2(c)]. In the same gate range at finite field $B = 0.3$ T [Fig. 2(d)], three oscillations around zero bias and higher bias subgap states are observed. At a higher field $B = 0.5$ T [Fig. 2(e)], an extended zero-bias peak is observed. Over a range of BG between 1.61 and 1.62 V the ZBP vanishes; however, this is an artifact due to charge jumps, i.e., charge rearrangements near the gate leading to a momentary shift in the electrostatic potential. Such charge jumps are also ubiquitous and appear in many published results [19].

We observe that the near-zero bias states often merge continuously into the transient resonances above the induced gap. This implies a relation between the two types of features. This behavior is expected in quantum dots strongly coupled to superconductors, where transport resonances due to ABS split from and merge into the induced gap as the dot occupation changes from even to odd [26,38]. In this framework, the regime in Fig. 2 is consistent with several coupled quantum dots formed near the superconductor. Note that the absence of Coulomb blockade suggests open quantum dots and transparent contact to the superconductor. The open dots may be connected both in series and in parallel.

To model our devices we perform 3D Schrödinger-Poisson calculations that incorporate geometric and electrostatic details of the experimental device [39]. The calculations naturally capture the multiband nature of the system and its highly inhomogeneous electrostatic potential, which turn out to be the crucial elements responsible for the ubiquitous zero-bias peaks. The inhomogeneity arises due to device geometry, while disorder is not included in the model. A detailed description of the model can be found in the conjoint theoretical paper [30].

First, we demonstrate that the model generates ubiquitous zero-bias peaks, as seen in the experiment, by calculating the differential conductance [40] as a function of the BG1 voltage. The results are shown in Fig. 3 (compare with Fig. 2). At zero magnetic field [Fig. 3(a)], the differential conductance is characterized by multiple subgap resonances that approach or cross zero bias without sticking. At finite field [Fig. 3(b)], one notices features that are confined near zero energy. Examples of differential conductance maps as a function of Zeeman energy and bias are shown in Figs. 3(c) and 3(d). In Fig. 3(c), we notice an in-gap mode that collapses to zero energy at $E_Z \approx 0.7$ meV, then splits at higher E_Z. A slight change in BG1 generates a

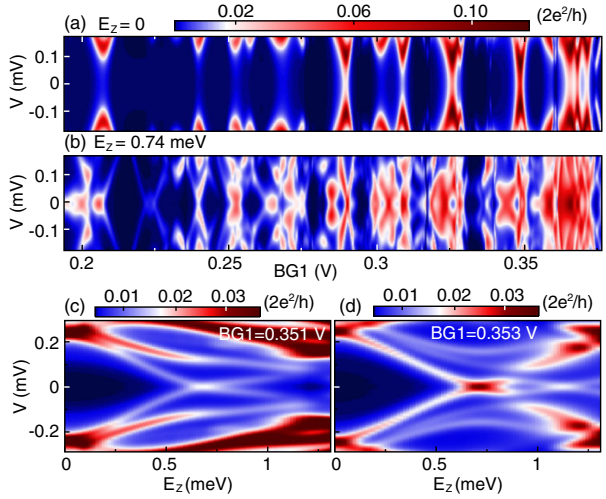

FIG. 3. Calculated differential conductance as a function of BG1 and bias voltage V for (a) $E_Z = 0$ and (b) $E_Z = 0.74$ meV. The FG voltage is 0.38 V and the temperature $k_BT = 0.15$ meV. [(c) and (d)] Calculated differential conductance as a function of Zeeman energy and bias voltage V for BG1 = 0.351 and 0.353 V, respectively.

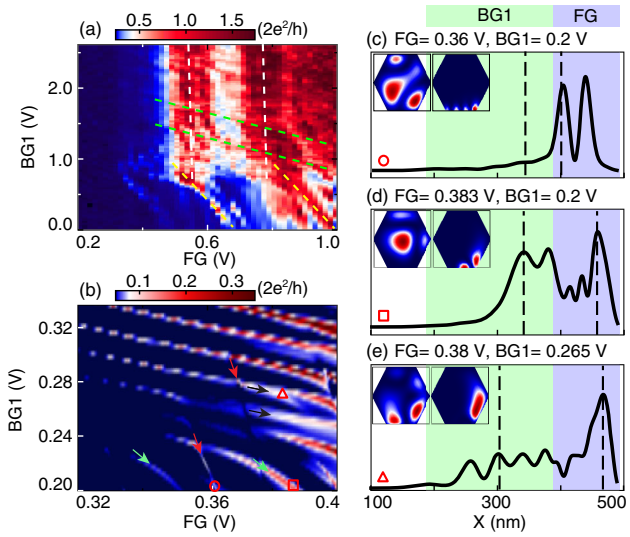

FIG. 4. (a) Measured and (b) calculated zero-bias voltage conductance at zero magnetic field as a function of FG and BG1. Note the three types of resonances characterized by different slopes [dashed lines in panel (a) and arrows in panel (b)]. [(c)–(e)] Calculated wave function profiles for the states marked in panel (b). The insets show the transverse profiles at the locations marked by black dashed lines. Regions of BG1 and FG are marked by green and purple shadows, respectively.

low-energy mode that remains near zero bias over a large range of E_z [Fig. 3(d)].

Next, we address the key question regarding the nature of the low-energy states by studying the band and real-space structure of the corresponding wave functions (also see Supplemental Material [41]). We find that the ubiquitous low-energy states are not MBS emerging in a segment of the wire, or partially separated MBS induced by soft confinement, but rather ABS pinned near zero energy by level repulsion. As detailed in the conjoint theory paper [30], interband coupling can give rise to ABS that stick near zero energy due to anticrossings between multiple modes approaching zero energy at different magnetic fields. For example, in Fig. 3(d) one can distinguish two low-energy modes that cross zero energy at $E_Z \approx 0.7$ meV and $E_Z \approx 1.1$ meV, respectively, displaying an anticrossing behavior (near $E_Z \approx 0.9$ meV). Evidence of similar level repulsion behavior can be found in the experimental results shown in Figs. 1(b) and 1(c). We note that the interband coupling arises from the evolution along the length of the wire of the transverse profiles of the various bands due to the electrostatic potential nonuniformity. As explained in the theory paper [30], single-sub-band models cannot capture this zero-bias pinning behavior for short nanowire segments of 200 nm (the width of BG1) without assuming overlapping MBS.

We investigate the spatial characteristics of the low-energy states at zero magnetic field by mapping the zero-bias conductance as a function of BG1 and FG. The experimental results are shown in Fig. 4(a), while the numerical results are given in Fig. 4(b). The remarkable common feature is the presence of three types of resonances characterized by different slopes. These resonances in the experiment and simulation may not appear exactly the same but have the same nature, which we attribute to distinct families of low-energy states with most of their wave function localized in different parts of the device. The nearly vertical resonances in Fig. 4(a) (white dashed lines) and Fig. 4(b) (red arrows) are generated by states coupled primarily to the FG gate. The wave function profile of a typical state associated with this type of resonance [Fig. 4(c)] reveals that most of its weight is located in the FG region (see the inset). The two additional sets of resonances are generated by states electrostatically coupled to both FG and BG1 [green and yellow dashed lines in panel (a), and black and green arrows in panel (b)]. As revealed by the wave function profiles shown in Figs. 4(d) and 4(e), these states have significant weight in both BG1 and FG regions. However, the transverse profiles (see the insets) show that the state in Fig. 4(e) is located closer to BG1 and farther away from FG as compared to the state in Fig. 4(d), which explains the different slopes of the corresponding resonances. The existence of these distinct families of states demonstrates that the low-energy physics is controlled by modes localized in different adjacent regions (i.e., the FG region and the covered and uncovered BG1 regions) that are coupled to one another. At finite magnetic field, this generically produces low-energy ABS resonances pinned near zero energy through the interband coupling mechanism discussed in detail in Ref. [30]. We note a discrepancy in

gate voltage and conductance scales between Fig. 4(a) and 4(b), likely as a result of device-dependent gate screening variations and high sensitivity of conductance to tunneling rates.

In conclusion, we have demonstrated that many of the commonly discussed features of MBS in nanowires, such as gap closing, zero-bias pinning in magnetic field or gate, and peak oscillations around zero bias, are ubiquitous and easily observed when ensembles of trivial ABS are present. Evidence of MBS in tunneling experiments should therefore be accompanied by detailed studies of subgap resonances in the extended gate voltage range. For example, an earlier study of a similar device has revealed zero-bias peaks occupying a large continuous region of field-gate space with a boundary similar to the basic topological condition [17].

Nevertheless, since tunneling measurements have so far not yielded a definite MBS proof, it is intuitively attractive to explore more sophisticated techniques, e.g., the fractional Josephson effect [43], Majorana fusion, or even braiding [44]. However, the added measurement complexity will not help resolve the experimental limitations of the tunneling experiments, since the limitations remain rooted in the growth and fabrication. It is also unclear whether advanced techniques can reveal signatures unique to MBS, and whether they are better at distinguishing MBS from ABS [45]. At the same time, tunneling remains powerful in surveying the subgap spectra in proximitized nanowires, thereby guiding device design and fabrication towards a more ideal regime in which MBS can be demonstrated unambiguously.

We thank V. Mourik and K. Zuo for comments on the manuscript. T. D. S. acknowledges NSF Grant No. DMR-1414683. S. M. F. acknowledges Grants No. NSF DMR-1743972 and No. NSF PIre1743717, ONR and ARO.

*frolovsm@pitt.edu

[1] L. Fu and C. L. Kane, Phys. Rev. Lett. **100**, 096407 (2008).
[2] J. Alicea, Phys. Rev. B **81**, 125318 (2010).
[3] J. D. Sau, S. Tewari, R. M. Lutchyn, T. D. Stanescu, and S. Das Sarma, Phys. Rev. B **82**, 214509 (2010).
[4] R. M. Lutchyn, J. D. Sau, and S. Das Sarma, Phys. Rev. Lett. **105**, 077001 (2010).
[5] Y. Oreg, G. Refael, and F. von Oppen, Phys. Rev. Lett. **105**, 177002 (2010).
[6] J. Alicea, Rep. Prog. Phys. **75**, 076501 (2012).
[7] C. Beenakker, Annu. Rev. Condens. Matter Phys. **4**, 113 (2013).
[8] N. Read and D. Green, Phys. Rev. B **61**, 10267 (2000).
[9] V. Mourik, K. Zuo, S. M. Frolov, S. Plissard, E. P. Bakkers, and L. P. Kouwenhoven, Science **336**, 1003 (2012).
[10] A. Das, Y. Ronen, Y. Most, Y. Oreg, M. Heiblum, and H. Shtrikman, Nat. Phys. **8**, 887 (2012).
[11] M. Deng, C. Yu, G. Huang, M. Larsson, P. Caroff, and H. Xu, Nano Lett. **12**, 6414 (2012).
[12] A. D. K. Finck, D. J. Van Harlingen, P. K. Mohseni, K. Jung, and X. Li, Phys. Rev. Lett. **110**, 126406 (2013).
[13] H. O. H. Churchill, V. Fatemi, K. Grove-Rasmussen, M. T. Deng, P. Caroff, H. Q. Xu, and C. M. Marcus, Phys. Rev. B **87**, 241401(R) (2013).
[14] S. Nadj-Perge, I. K. Drozdov, J. Li, H. Chen, S. Jeon, J. Seo, A. H. MacDonald, B. A. Bernevig, and A. Yazdani, Science **346**, 602 (2014).
[15] S. M. Albrecht, A. P. Higginbotham, M. Madsen, F. Kuemmeth, T. S. Jespersen, J. Nygård, P. Krogstrup, and C. M. Marcus, Nature (London) **531**, 206 (2016).
[16] M. T. Deng, S. Vaitiekenas, E. B. Hansen, J. Danon, M. Leijnse, K. Flensberg, J. Nygård, P. Krogstrup, and C. M. Marcus, Science **354**, 1557 (2016).
[17] J. Chen, P. Yu, J. Stenger, M. Hocevar, D. Car, S. R. Plissard, E. P. A. M. Bakkers, T. D. Stanescu, and S. M. Frolov, Sci. Adv. **3**, e1701476 (2017).
[18] Ö. Gül, H. Zhang, J. D. Bommer, M. W. de Moor, D. Car, S. R. Plissard, E. P. Bakkers, A. Geresdi, K. Watanabe, T. Taniguchi *et al.*, Nat. Nanotechnol. **13**, 192 (2018).
[19] H. Zhang *et al.*, Nature (London) **556**, 74 (2018).
[20] H. J. Suominen, M. Kjaergaard, A. R. Hamilton, J. Shabani, C. J. Palmstrøm, C. M. Marcus, and F. Nichele, Phys. Rev. Lett. **119**, 176805 (2017).
[21] F. Nichele, A. C. C. Drachmann, A. M. Whiticar, E. C. T. O'Farrell, H. J. Suominen, A. Fornieri, T. Wang, G. C. Gardner, C. Thomas, A. T. Hatke, P. Krogstrup, M. J. Manfra, K. Flensberg, and C. M. Marcus, Phys. Rev. Lett. **119**, 136803 (2017).
[22] E. J. H. Lee, X. Jiang, R. Aguado, G. Katsaros, C. M. Lieber, and S. De Franceschi, Phys. Rev. Lett. **109**, 186802 (2012).
[23] D. I. Pikulin, J. P. Dahlhaus, M. Wimmer, H. Schomerus, and C. W. J. Beenakker, New J. Phys. **14**, 125011 (2012).
[24] M. Popinciuc, V. E. Calado, X. L. Liu, A. R. Akhmerov, T. M. Klapwijk, and L. M. K. Vandersypen, Phys. Rev. B **85**, 205404 (2012).
[25] K. Zuo, V. Mourik, D. B. Szombati, B. Nijholt, D. J. van Woerkom, A. Geresdi, J. Chen, V. P. Ostroukh, A. R. Akhmerov, S. R. Plissard, D. Car, E. P. A. M. Bakkers, D. I. Pikulin, L. P. Kouwenhoven, and S. M. Frolov, Phys. Rev. Lett. **119**, 187704 (2017).
[26] E. J. Lee, X. Jiang, M. Houzet, R. Aguado, C. M. Lieber, and S. De Franceschi, Nat. Nanotechnol. **9**, 79 (2014).
[27] G. Kells, D. Meidan, and P. W. Brouwer, Phys. Rev. B **86**, 100503(R) (2012).
[28] C. Moore, T. D. Stanescu, and S. Tewari, Phys. Rev. B **97**, 165302 (2018).
[29] A. Vuik, B. Nijholt, A. Akhmerov, and M. Wimmer, arXiv: 1806.02801.
[30] B. D. Woods, J. Chen, S. M. Frolov, and T. D. Stanescu, companion paper, Phys. Rev. B **100**, 125407 (2019).
[31] P. Krogstrup, N. L. B. Ziino, W. Chang, S. M. Albrecht, M. H. Madsen, E. Johnson, J. Nygård, C. M. Marcus, and T. S. Jespersen, Nat. Mater. **14**, 400 (2015).
[32] J. Shabani, M. Kjaergaard, H. J. Suominen, Y. Kim, F. Nichele, K. Pakrouski, T. Stankevic, R. M. Lutchyn, P. Krogstrup, R. Feidenhans'l, S. Kraemer, C. Nayak, M. Troyer, C. M. Marcus, and C. J. Palmstrøm, Phys. Rev. B **93**, 155402 (2016).

[33] S. Gazibegovic *et al.*, Nature (London) **548**, 434 (2017).
[34] S. M. Albrecht, A. P. Higginbotham, M. Madsen, F. Kuemmeth, T. S. Jespersen, J. Nygård, P. Krogstrup, and C. M. Marcus, Nature (London) **531**, 206 (2016).
[35] A. Vuik, D. Eeltink, A. Akhmerov, and M. Wimmer, New J. Phys. **18**, 033013 (2016).
[36] T. D. Stanescu, R. M. Lutchyn, and S. Das Sarma, Phys. Rev. B **87**, 094518 (2013).
[37] I. van Weperen, S. R. Plissard, E. P. A. M. Bakkers, S. M. Frolov, and L. P. Kouwenhoven, Nano Lett. **13**, 387 (2013).
[38] A. Eichler, M. Weiss, S. Oberholzer, C. Schönenberger, A. Levy Yeyati, J. C. Cuevas, and A. Martín-Rodero, Phys. Rev. Lett. **99**, 126602 (2007).
[39] B. D. Woods, T. D. Stanescu, and S. Das Sarma, Phys. Rev. B **98**, 035428 (2018).
[40] G. E. Blonder, M. Tinkham, and T. M. Klapwijk, Phys. Rev. B **25**, 4515 (1982).
[41] See Supplemental Material at http://link.aps.org/supplemental/10.1103/PhysRevLett.123.107703 for more data and discussions, which includes Refs. [26,39,42].
[42] S. Vaitiekénas, M.-T. Deng, J. Nygård, P. Krogstrup, and C. M. Marcus, Phys. Rev. Lett. **121**, 037703 (2018).
[43] L. P. Rokhinson, X. Liu, and J. K. Furdyna, Nat. Phys. **8**, 795 (2012).
[44] D. Aasen, M. Hell, R. V. Mishmash, A. Higginbotham, J. Danon, M. Leijnse, T. S. Jespersen, J. A. Folk, C. M. Marcus, K. Flensberg, and J. Alicea, Phys. Rev. X **6**, 031016 (2016).
[45] M. Houzet, J. S. Meyer, D. M. Badiane, and L. I. Glazman, Phys. Rev. Lett. **111**, 046401 (2013).